Journal of Catalysis **185,** 435–444 (1999)
Article ID jcat.1999.2476, available online at http://www.idealibrary.com on IDEAL®

Comparative Evaluation of the Catalytic Properties of SAPO-31 and ZSM-48 for the Hydroisomerization of *N-Octane*: Effect of the Acidity

P. Mériaudeau,[1] Vu A. Tuan, Vu T. Nghiem, G. Sapaly, and C. Naccache

Institut de Recherches sur la Catalyse, CNRS, 2 Avenue Albert Einstein, 69626 Villeurbanne Cedex, France

Received December 17, 1998; revised March 4, 1999; accepted March 6, 1999

The hydroconversion of *n*-octane, 2-methylheptane, and 2,2,4-trimethylpentane over Pt–Pd/SAPO-31 and Pt–Pd/ZSM-48 at 523 K and atmospheric pressure was studied. The acid SAPO-31 and ZSM-48 supports were synthesized by hydrothermal procedures and characterized by X ray, scanning electron microscopy, and MAS-NMR. Infrared spectra of adsorbed pyridine showed that these molecular sieves differ in their acidity not by the number of acid sites but by their strength. The bifunctional catalysts Pt–Pd/SAPO-31 and Pt–Pd/ZSM-48 were highly selective for the hydroisomerization of *n*-octane. Monomethyl isomers were the major products. These narrow tubular molecular sieves favored the formation of terminal methyl isomers $2MeC_7$ and 2,5DMe-C_6. Acid strength has almost no effect on the hydroisomerization selectivity, but high acid strength led to a higher reaction rate. Isomerization of 2-methylheptane into $3MeC_7$ by 1,2-methyl shift or into *n*-C_8 by PCP intermediate discriminates molecular sieves having channels of different diameters, the smaller the dimensions of the pores the lower the ratio of $3MeC_7$/*n*-C_8.

Key Words: **hydroisomerization; *n*-octane; SAPO-31; ZSM-48.**

INTRODUCTION

The skeletal isomerization of linear alkanes over bifunctional catalysts is accompanied by the formation of multibranched isomers which undergo facile fragmentation through favorable β-scission pathways. As a consequence, over classical bifunctional catalysts the isomerization yield never reaches high values. Recently it has been shown that bifunctional catalysts, containing a noble metal, Pd or Pt, on a medium-pore molecular sieve, such as SAPO-11 (1) and ZSM-22 (2), have high selectivity for long-chain alkane hydroisomerization. A new process for lowering the pour point of high wax feeds has been developed (3). SAPO-11 and ZSM-22 contain parallel, elliptical, 10-membered rings, nonintersecting tubular pores with cross section diameters of 0.39×0.63 and 0.45×0.55 nm, respectively. The peculiar topology of SAPO-11 and ZSM-22 is responsible for the observed high hydroisomerization selectivity. Transition state shape selectivity has been invoked to explain such high selectivity for hydroisomerization (1–6). According to the classical mechanism for skeletal isomerization, substituted corner protonated cyclopropyl carbonium intermediates are formed at the pore mouths (4–6) of the molecular sieves. In the branching reaction, particularly in the monobranching step, it was argued that only part of the molecule penetrates the micropore (5, 6). However, other authors provided evidence that monobranching through protonated cyclopropane intermediates (PCP) followed by ring opening occurred inside the pore at the pore mouth and a short distance from the grain surface (4, 7). All of these works have essentially put emphasis on the topology of the molecular sieves, with little consideration of the acidity parameter. In (1) it was concluded that the one-dimensional nature of the pores in SAPO-11, the narrow sizes, and the moderate acid activity contribute to the excellent performance in branching reactions.

Silicoaluminophosphates (SAPO) generally have a lower acidity than zeolites (8). Comparison of the behavior of bifunctional catalysts based on a SAPO molecular sieve to that of catalysts based on zeolite would permit an approach to the role of the acidity in the hydroisomerization reaction, provided that the SAPO and the zeolite have identical pore topology and dimension. SAPO-31 has the ATO structure type with nonintersecting 12-membered ring channels with a cross section of 0.54 nm (9). The framework topology of ZSM-48 contains 10-membered ring, non-interpenetrating linear channels whose dimensions are 0.53×0.56 nm (10). These two molecular sieves are particularly suitable for investigating the effect of the support acidity of medium tubular pore molecular sieves on the hydroisomerization of alkanes.

EXPERIMENTAL

Materials

SAPO-31 was synthesized hydrothermally according to the established procedure. Pseudo-boehmite (catapal B

[1] To whom correspondence should be addressed.

0021-9517/99 $30.00

vista) was added to a solution containing phosphoric acid (85%) under vigorous strirring for 3 h. To this mixture, the template di-*n*-propylamine, the source of silicon, tetraethylorthosilicate in hexanol, and a surfactant, dodecylamine, were added under stirring. The microemulsion thus obtained was poured into a Teflon container which was put in an autoclave. The gel mixture in the autoclave was continuously stirred while the whole system was heated to 473 K. The crystallization time was 48 h. The white solid crystalline product recovered by centrifugation was carefully washed with distilled water, dried at 393 K for 3 h, and then calcined at 873 K for 5 h to remove all organic compounds. The hydrogel had the following molar composition:

$$0.83\ Al_2O_3;\ 1\ P_2O_5;\ 0.5\ SiO_2;\ 1\ Pr_2NH;\ 0.14\ (CH_3)_2NH_2,$$
$$4.4\ \text{hexanol};\ 40\ H_2O.$$

The synthesis of ZSM-48 was as follows. Fumed silica was added to an aqueous solution of NaOH (Merck) (90 wt% H_2O of total amount of H_2O used for the synthesis) under vigorous stirring. To this solution, pyrrolidine (Fluka) as the template, $Al(NO_3)_3$, $9H_2O$ (Merck) dissolved in H_2SO_4 (98%), and H_2O (remaining 10%) were added. The hydrogel was stirred for 3 h at room temperature, transferred into a Teflon flask, and then put in the autoclave heated at 453 K. The crystallization was carried out for 48 h under stirring conditions. The white powder was recovered by centrifugation, washed with distilled water, dried at 393 K, and finally calcined at 823 K under oxygen for 10 h. H-form ZSM-48 was obtained by NH_4^+ ion exchange followed by calcination at 773 K for 3 h. The hydrogel had the following molar composition: 0.5 Al_2O_3; 110 SiO_2; 43 NaOH; 20 H_2SO_4; 50 pyrrolidine, 5000 H_2O.

Bifunctional catalysts were obtained by impregnating SAPO-31 and H-ZSM-48 successively with Pt and Pd solutions, to obtain metal loadings on each sample of 0.6 wt% Pt and 1.2 wt% Pd. The metal-loaded samples were calcined under oxygen at 673 K prior to reduction and finally reduced under H_2 at 773 K.

Characterization

X-ray diffraction patterns were recorded on a Philips PW 1050 diffractometer using Cu$K\alpha$ radiation.

Scanning electron micrographs were obtained on a Hitachi S800 scanning electron microscope.

The ^{27}Al, ^{29}Si, and ^{31}P MAS-NMR spectra were recorded on a Brucker DSX 400 spectrometer. Chemical shifts were measured relative to 85% aq H_3PO_4 for ^{31}P, $Al(NO_3)_3$ for ^{27}Al, and tetramethylsilane for ^{29}Si. ^{27}Al NMR spectra were obtained using a pulse length of 1 μs and a recycle delay of 1s.

The Al and P contents of the samples were determined by atomic adsorption spectroscopy after dissolution of the solid. The Si content was calculated by difference. The chemical composition of SAPO-31 powder was (in wt%): 20.7 Al, 23.4 P, 2.3 Si, and Si/Al = 116 for ZSM-48. Infrared spectra were recorded on a Brucker FT spectrometer. The powder was pressed into thin wafers, which were activated under vacuum in a special cell. The cell allowed *in situ* infrared measurements under controlled atmosphere.

Catalytic Measurements

The catalytic reactions were carried out using a quartz tubular flow microreactor. All experiments were done at 523 K and 1 bar. The catalysts (100–200 mg) were activated in a pure hydrogen stream at 773 K in the reactor. The weight hourly space velocity (WHSV) was varied by changing the flow rate of the feed. WHSV was varied in the range 0.02–22 h^{-1}. The feed and the products were analyzed online using a gas chromatograph fitted with a flame ionization detector. The chromatographs were equipped with a Pona capillary column (Altech France) for C_8 alkanes and with an Unibead 3S column (Altech, France) for analyzing the cracked products. The relative rates of reaction are given by the quantity $\alpha \times$ WHSV, where α is the conversion of the alkane in wt% and WHSV is the space velocity in h^{-1}. These relative reaction rates were determined at low conversion, generally less than 10%. The feeds (Aldrich), *n*-octane (*n*-C_8), 2-methylheptane (2MeC_7), and 2,2,4-trimethylpentane (2,2,4TMP), were used without further purification.

RESULTS AND DISCUSSION

Characterization

SAPO-31. Figure 1a shows the X-ray diffraction pattern of the silicoaluminophosphate material. It is identical to the powder pattern of conventionally synthesized SAPO-31 (9) except for the presence of an extra peak due to a crystobalite impurity ($2\theta = 22^\circ$).

The ^{27}Al and ^{31}P MAS-NMR spectra of the silicoaluminophosphate sample, not shown in this paper, contained sharp resonances near 36 ppm for ^{27}Al and -29 ppm for ^{31}P. These chemical shifts are typical for aluminophosphate molecular sieves (8, 9, 11) and confirm the tetrahedral crystallographic positions of aluminum and phosphorous with a strict alternation of Al and P atoms at T positions of the SAPO framework.

Figure 2 shows the ^{29}Si MAS-NMR spectrum of the SAPO sample under study. Silicon incorporation in the framework is derived from the examination of the spectrum which has been deconvoluted into at least three major resonance peaks at -110, -103, and -95 ppm and possibly another peak at -116 ppm.

The peak with maxima around -95 ppm has been ascribed to silicon atoms incorporated in the aluminophosphate framework on phosphorous T sites, each silicon atom in the framework being bonded via oxygen to four

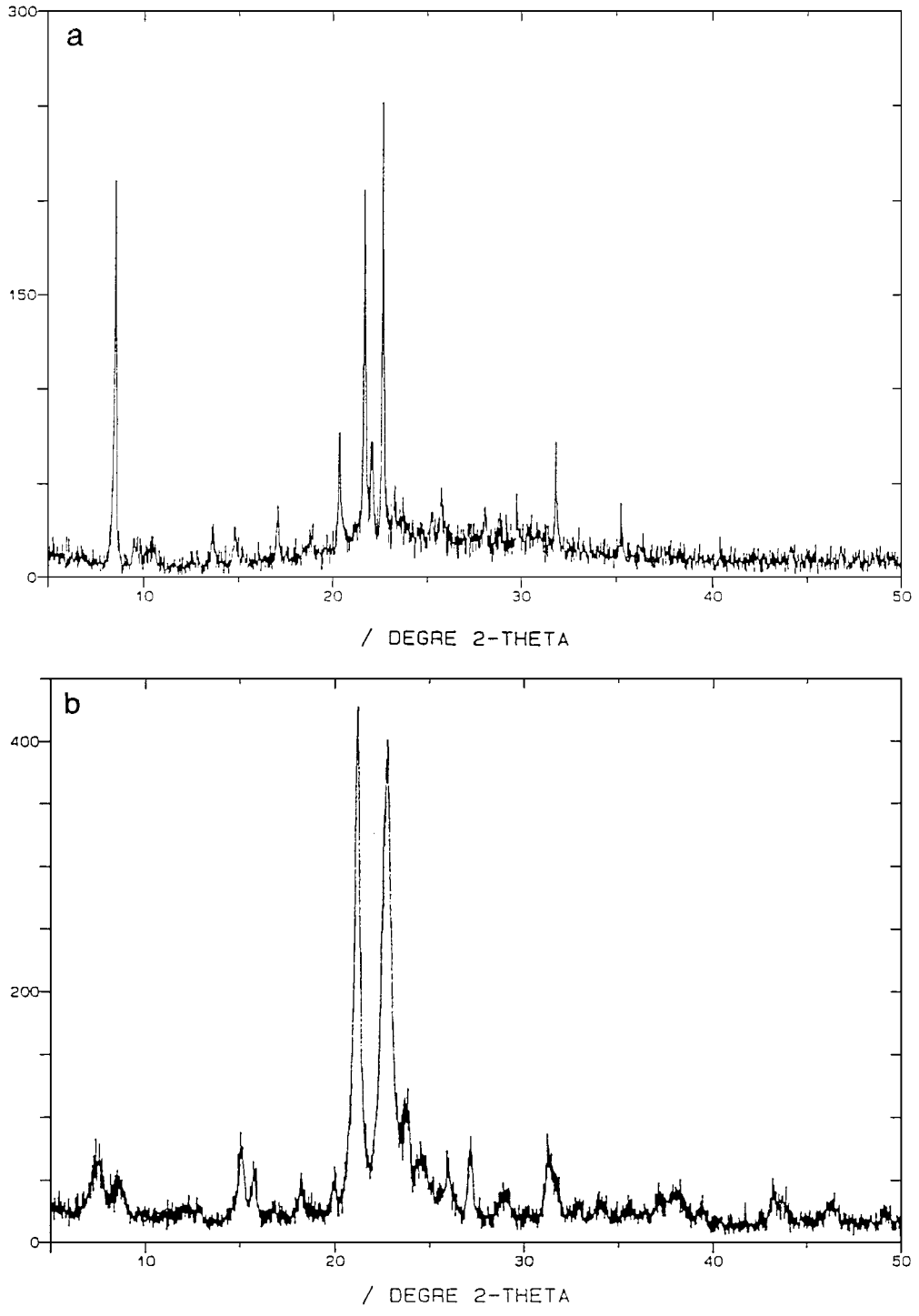

FIG. 1. (a) X-ray powder pattern of SAPO-31. (b) X-ray powder pattern of ZSM-48.

aluminum atoms (12, 13). Each silicon atom incorporated in this way causes a Brønsted acid site. The second peak at −110 ppm represents silicon atoms bonded via oxygen to four silicon atoms. This signal has been attributed either to silica-rich islands in the silicoaluminophosphate framework when two Si atoms replace simultaneously one Al and one P on T sites or to silicon in silica by products (13–15). From the deconvolution and the integration of the peaks at −110 and −116 ppm it is estimated that around 50% of the silicon atoms are located in a pure silica domain where no Brønsted acidity is generated. The peak at −95 ppm corresponds to approximatively 20% of the total silicon atoms. The signal at −103 ppm has been observed on Si-rich SAPO-37 and possibly attributed to Si (1 Al, 3 Si) in

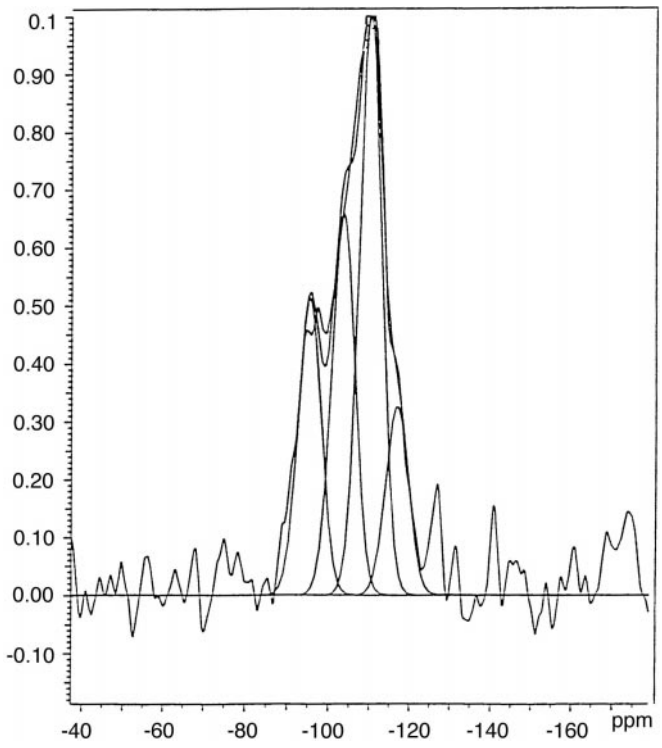

FIG. 2. Experimental and deconvoluted ^{29}Si MAS-NMR spectra of SAPO-31.

a silica-alumina intergrowth domain or at the interface of the silica and the AlPO domains (12). However, ^{27}Al MAS-NMR studies have never revealed a peak around 60 ppm as observed for pure aluminosilicate molecular sieves (zeolites).

The X-ray diffraction and MAS-NMR studies of the silicoaluminophosphate sample clearly demonstrate that well-crystallized SAPO-31 material has been synthesized; however, in this silicon-rich SAPO-31 sample only a fraction of the Si atoms were in the SAPO domain Si (4Al).

A scanning electron micrograph of SAPO-31 is shown in Fig. 3a. Shaped crystals are distinguished. The crystals are thin with more or less eroded edges. The length of these sheet-like crystals is in the range 1–2 μm.

ZSM-48. The aluminosilicate, silica-rich material, synthesized in this work presents the X-ray powder pattern shown in Fig. 1b. All observed X-ray powder lines are consistent with the X-ray powder pattern of ZSM-48 free from impurities (10), but with different relative peak intensities.

A scanning electron micrograph of the synthesized ZSM-48 crystal is shown in Fig. 3b. Fibrous rods or needles with a length of about 0.75 μm and a diameter of 0.07 μm were formed as compared to the fibrous rods of ZSM-48 with a diameter of about 1 μm and a length of 4–5 μm found in (16).

The ^{27}Al MAS-NMR spectrum of the calcined sample displays a peak at 50–60 ppm, which corresponds to framework aluminum. No peak at 0 ppm is observed, which indicates the absence of nonframework aluminum on this silicon-rich ZSM-48 (Fig. 4).

Brønsted acidity of SAPO-31 compared to the acidity of ZSM-48. Figure 5a shows the IR spectra of SAPO-31 which has been outgassed at 673 K before and after pyridine adsorption. In the region of the OH stretching vibrations, an hydroxyl IR band at about 3620 cm^{-1} is observed. The OH responsible for this band could be present in the SAPO domain, at the boundary between the silica and the SAPO domains, or in the SA domain (17).

The band at 3620 cm^{-1} was broad and had a low intensity. In addition to this IR band, two additional IR bands were observed, an intense one at 3675 cm^{-1} attributed to P–OH groups and one at 3740 cm^{-1} with low intensity assigned either to Al–OH or to Si–OH groups on the grain surface. In conclusion, in the SAPO-31 under study silicon substituted for phosphorous in the framework generated SiO(H)Al groups comparable to those existing in zeolites when the bridging character of hydroxyls is considered. In agreement with the ^{29}Si MAS-NMR results, the concentration of these Brønsted sites is low as jugded from the low intensity of the IR band.

The ZSM-48 sample was also examined by IR in the OH stretching region. A broad low intensity IR band centered around 3600 cm^{-1} was detected (Fig. 5b).

A comparative study of the respective acidity of SAPO-31 and ZSM-48 was made possible from the IR spectra of pyridine adsorbed on these samples. Figure 5 shows that upon pyridine adsorption on SAPO-31 at room temperature and subsequent outgassing at 373 K the IR bands at 3620 and 3675 cm^{-1} disappeared. Upon outgassing the sample at 473 K the band at 3675 cm^{-1} was almost completely restored and at 573 K the IR band at 3620 cm^{-1} was also restored. These IR results indicate that both P–OH and SiO(H)Al groups interact with pyridine through acid-base reactions, which are easily reversible for P–OH and SiO(H)Al Brønsted acid sites.

Figures 6 and 7 represent the IR spectra of pyridine adsorbed on SAPO-31 and ZSM-48, respectively. These spectra are characteristic of pyridine adsorbed on Brønsted acid sites forming pyridinium ions (1550 cm^{-1}) and of pyridine coordinatively bonded to Lewis acid sites (1450 cm^{-1}).

From the intensities of the IR band at 1450 cm^{-1} attributed to pyridine coordinatively bonded to Lewis acid sites and of the IR band at 1550 cm^{-1} due to pyridinium ions, the acidities of SAPO-31 and ZSM-48 were determined and compared. In agreement with the IR study of SAPO-31 in the OH stretching region, Fig. 6 indicates that pyridinium ions formed on SAPO-31 completely decomposed upon outgassing at 573 K, the IR band at 1550 cm^{-1} being erased after this treatment. It is clear that SAPO-31 possesses a mild acid strength.

Figure 7 indicates that upon pyridine adsorption the IR band at 1550 cm^{-1} characteristic of pyridinium ions was

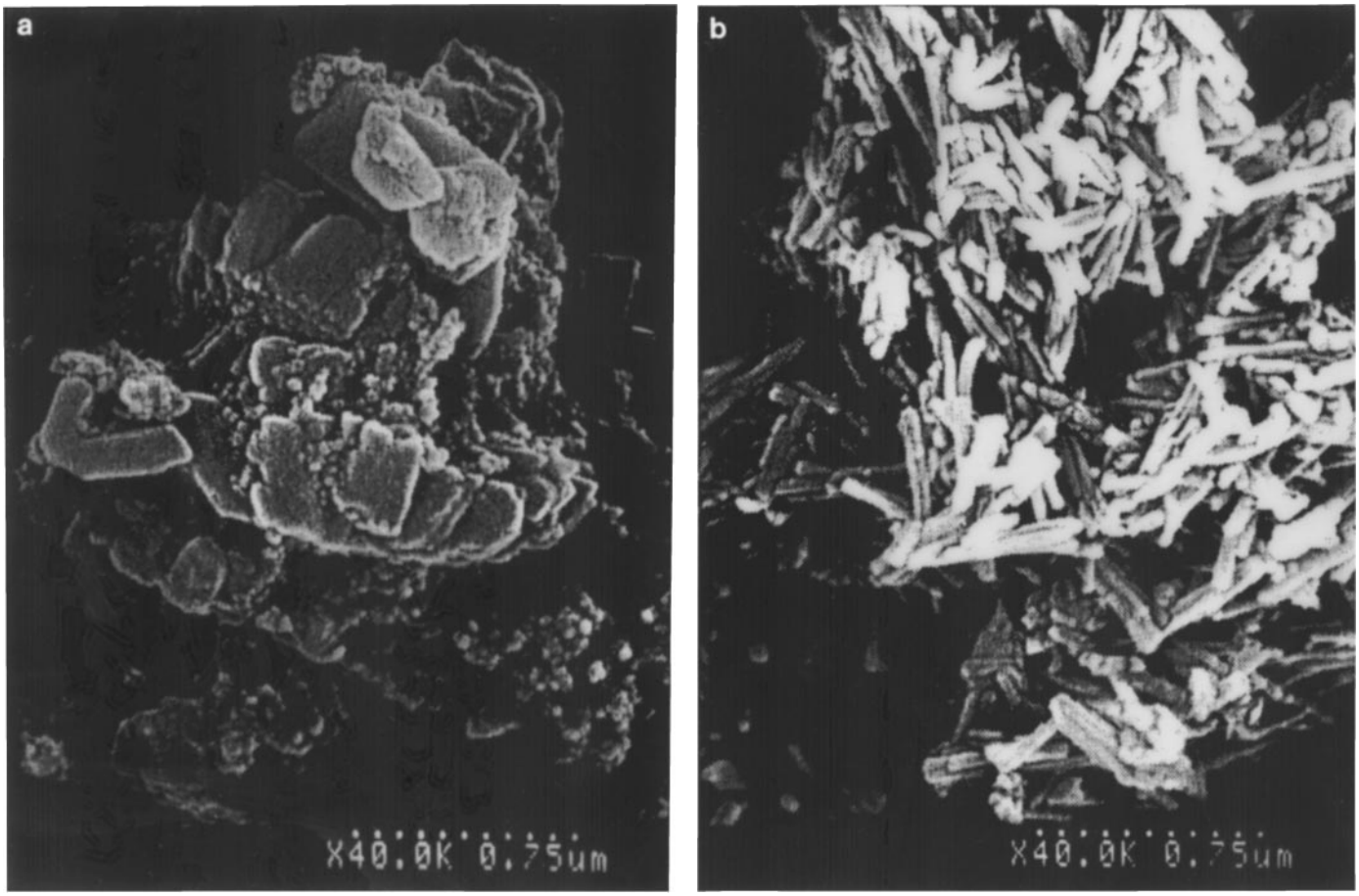

FIG. 3. (a) SEM of SAPO-31 and (b) SEM of ZSM-48.

observed, which indicates that Brønsted acid sites were indeed present on ZSM-48. The intensity of this IR band remained almost unchanged after outgassing the sample up to 573 K. The high stability of the pyridinium ions formed on ZSM-48 indicates that the acid strength of ZSM-48 is high. It is only upon outgassing the sample at 773 K that pyridinium ions were completely removed from the surface. Quantification of the Brønsted acidity on SAPO-31 and ZSM-48 was made possible, although not very accurate, by a comparison of the intensities of the IR bands at 1550 cm^{-1}. Since the weight of the SAPO-31 and ZSM-48 wafers was almost the same, Figs. 6 and 7 suggest that the number of Brønsted acid sites on SAPO-31 is comparable to that on ZSM-48. Since, it was noted above that no OH groups vibrating in the range of 3600 cm^{-1} were observed, this suggests that the OH group vibration is probably too large (not to weak) to be detected. However, the Brønsted acid sites on ZSM-48 are considerably stronger.

Catalytic Reactions

The true bifunctional behavior of the Pt–Pd/SAPO-31 and Pt–Pd/ZSM-48 catalysts will be treated first. A higher selectivity for hydroisomerization and pure primary hydrocracking are obtained when a strong hydrogenation function is present, the metal exhibiting the minimum hydrogenolysis activity. In order to verify that the catalysts were ideal bifunctional catalysts, the distribution of the cracked products from the hydrocracking of *n*-octane was determined. Figures 8 and 9 represent the distributions of the cracked products from the hydroconversion of *n*-C_8 over Pt–Pd/SAPO-31 and Pt–Pd/ZSM-48 at low and high conversions. With both catalysts C_1 and C_2 cracked products were present in a very small concentration with respect to the other cracked products.

The hydrogenolysis reaction of *n*-C_8 on the bimetallic Pt–Pd hence contributed little to the overall cracking of the alkane (18). Figures 8 and 9 furthermore show that the cracked products are symmetrically distributed around the C_4 fraction, which suggests that secondary hydrocracking reactions were not occurring. In addition the effect of the H_2 pressure on the *n*-octane reaction rate was investigated. It appeared on both catalysts that the *n*-C_8 conversion changed linearly with the reciprocal value of the hydrogen pressure $1/P_{H_2}$ in agreement with the hydrocracking model where at any H_2 pressure the alkane is in

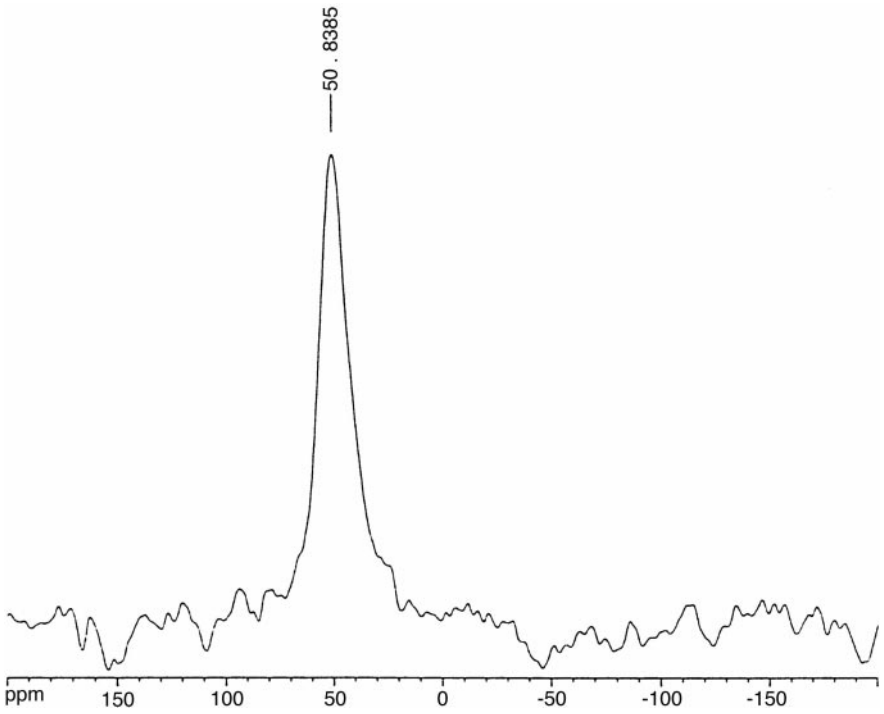

FIG. 4. ^{27}Al MAS-NMR spectrum of ZSM-48.

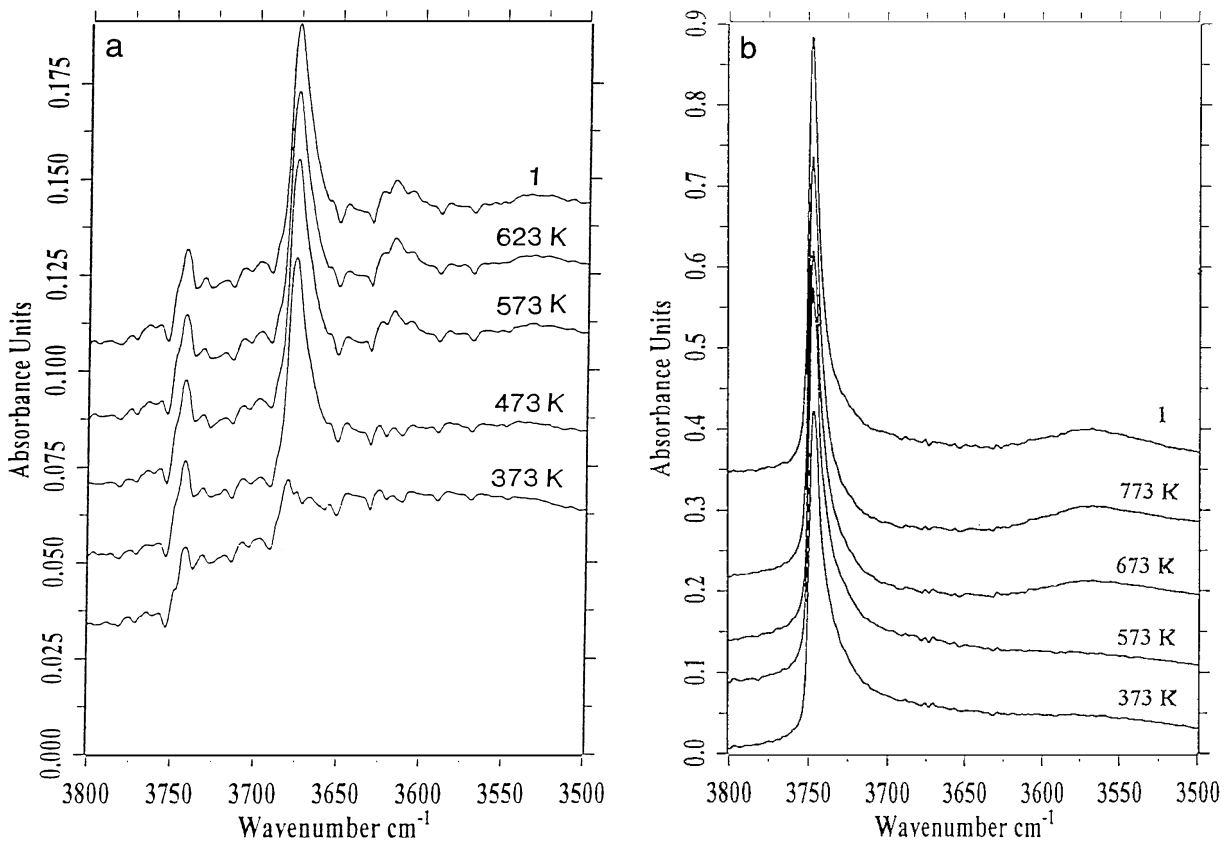

FIG. 5. (a) IR spectra in the OH stretching vibrations of SAPO-31 (1) sample outgassed at 673 K. Other spectra: sample outgassed at 673 K and after pyridine adsorption and desorption at increasing temperatures. (b) IR spectra in OH stretching vibrations of ZSM-48. (1) Sample outgassed at 773 K. Other spectra: sample outgassed at 773 K and after pyridine adsorption and desorption at increasing temperatures.

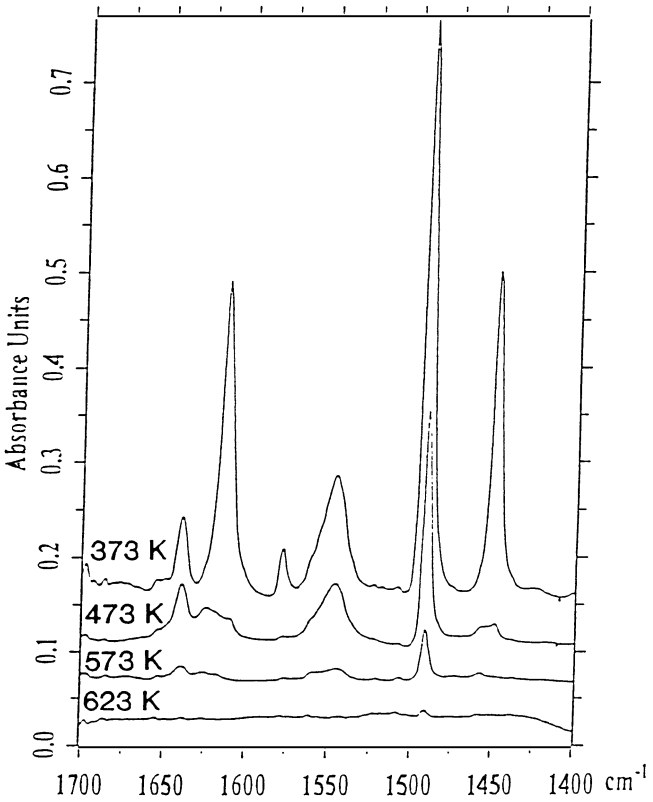

FIG. 6. IR spectra of pyridine adsorbed on SAPO-31 and desorbed at increasing temperatures.

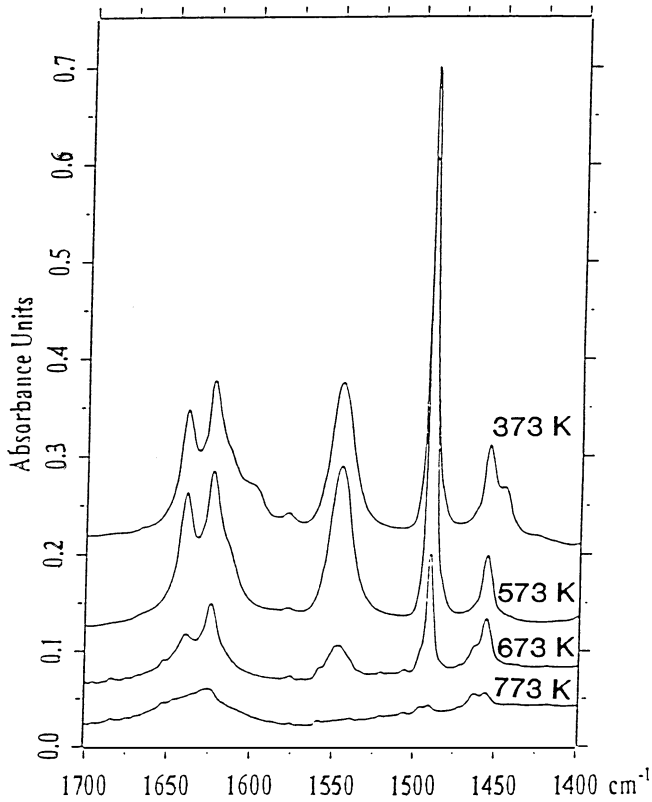

FIG. 7. IR spectra of pyridine adsorbed on H-ZSM-48 and desorbed at increasing temperatures.

equilibrium with the corresponding olefin. We conclude that Pt–Pd/SAPO-31 and Pt–Pd/ZSM-48 behave like true bifunctional catalysts.

The hydroconversion of *n*-octane obtained at 523 K led essentially to isomerized products; among them the monomethyl-branched isomers are the most abundant. C_8 isomer yields versus *n*-C_8 conversion over Pt–Pd/SAPO-31 and Pt–Pd/ZSM-48 are shown in Fig. 10. It is clear that both catalysts were highly selective for skeletal isomerization of *n*-alkane. An isomer yield of 78% at 80–85% *n*-C_8 conversion was reached for both materials. This means that over these medium tubular pore molecular sieves, the selectivity toward isomerization was not controlled by the acid strength of the catalyst. Apparently the stronger acidity of H-ZSM-48 did not induce more cracking of the feed as compared to SAPO-31.

However, as shown in Tables 1 and 2, a small difference exists between SAPO-31 and ZSM-48. At constant conversion, ZSM-48 gave less dimethylhexane isomers and more cracked products than SAPO-31. The explanation should be found in the longer effective residence time of the intermediate carbenium ions on the stronger acid sites present on ZSM-48. As a result, the probability that a cracking event will occur is higher over ZSM-48 than over SAPO-31. With the rates of cracking of dibranched carbenium ions higher than that of monobranched intermediates, dimethylhexane isomers will be preferentially cracked and hence ZSM-48 will give less dibranched isomers than SAPO-31. The distributions of the monomethylheptane isomers (Me-C_7) and dimethylhexanes ($DMeC_6$) at increasing *n*-octane conversion are shown in Table 1 and Table 2 for both catalysts.

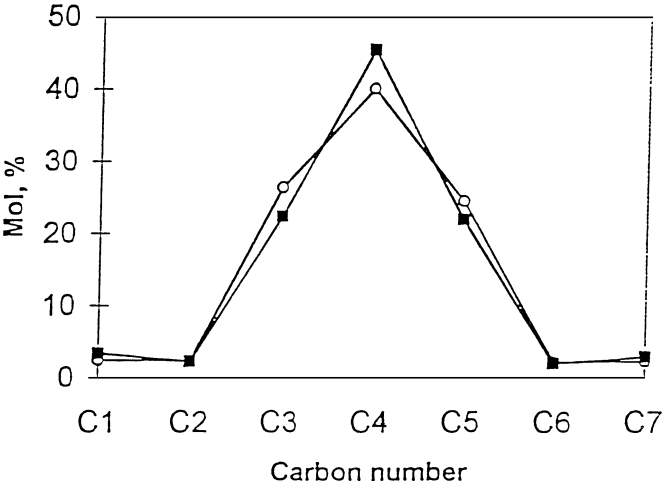

FIG. 8. *n*-Octane hydroconversion. Distribution of the cracked products over Pt–Pd/SAPO-31 at 523 K, 1 atm, H_2/HC = 60, (○) $\alpha = 11.3\%$, (■) $\alpha = 80.3\%$.

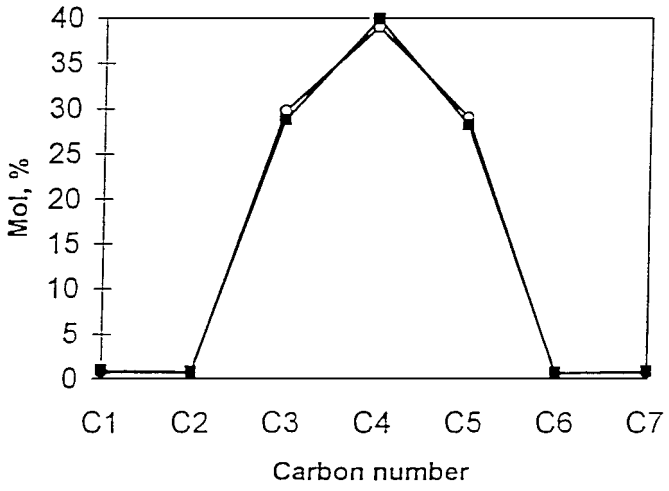

FIG. 9. *n*-Octane hydroconversion. Distribution of the cracked products over Pt–Pd/ZSM-48 at 523 K, 1 atm, H_2/HC = 60, (○) $\alpha = 10.3\%$, (■) $\alpha = 81.6\%$.

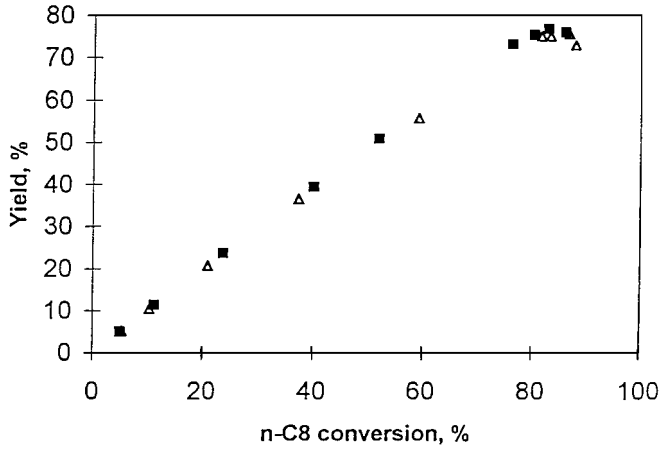

FIG. 10. *n*-Octane hydroconversions: C_8 isomer yield versus conversion, (△) Pt–Pd/ZSM-48, (■) Pt–Pd/SAPO-31.

As stated above Tables 1 and 2 show that monomethylheptane isomers were strongly favored, dimethylhexanes being formed significantly only at *n*-C_8 conversions above 80%. The distributions of Me-C_7 and DMe-C_8 were quite similar over SAPO-31 and H-ZSM-48. These results suggest that the acid strength not only has no effect on the overall selectivity for isomerization but also does not influence the respective isomer distributions. An interesting aspect of the results shown in Tables 1 and 2 is the predominant formation, within the isomer products, of terminally branched methyl isomers. At low conversion these isomers are formed beyond the amounts predicted by thermodynamics. The preferential formation of $2MeC_7$ and 2,5 $DMeC_6$ over medium noninterconnecting tubular pore molecular sieves was explained by the concept of restricted transition state shape selectivity at the pore mouth (4, 7). Apparently over SAPO-31 and H-ZSM-48 the selectivity for isomerization and the C_8 isomer distribution resulted from the stereochemistry imposed by the pore mouths rather than by the energetic chemistry imposed by the acid strength.

The hydroconversion and hydrocracking reactions which are consecutive reactions proceed essentially through carbenium ions, these ions being formed by protonation of the olefin formed by dehydrogenation of the alkane on the metal. With *n*-octane, branching of the *n*-octyl intermediate involves the formation of the corner-protonated cyclopropane intermediate. Within the restricted space available in the pore mouth of SAPO-31, terminal PCP intermediates are preferentially formed. Thus terminal monobranched methyl isomers are formed in agreement with the results given in Tables 1 and 2. In general high cracking rates were observed when multibranched isomers were formed and in particular with *n*-octane when trimethylpentanes were formed. Within SAPO-31 and ZSM-48, trimethylpentanes are too bulky and could not form within the pores; thus the cracking reaction is limited and the selectivity toward isomerization high.

TABLE 1

***n*-Octane Conversion on Pt–Pd-SAPO-31**

n-C_8 conversion, %	5.0	11.3	23.8	40.2	52.0	76.4	80.3	82.8	86.0
Cracking selectivity, %	0.1	0.4	1.0	2.0	2.4	4.4	6.2	7.3	11.7
iC_8 selectivity, %	99.9	99.6	99.0	97.9	97.6	95.6	93.7	92.6	88.2
MC selectivity, %	99.9	99.5	97.7	95.2	93.1	83.7	77.6	73.7	65.1
DMC_6 selectivity, %	—	0.1	1.3	2.7	4.5	11.9	16.1	18.9	23.0
MC_7 distribution, mol%									
$2MC_7$	48.1	47.1	46.5	45.9	45.2	43.6	42.7	41.5	39.8
$3MC_7$	43.7	44.1	44.4	44.6	44.6	45.7	46.0	46.5	46.8
$4MC_7$	8.2	8.8	9.2	9.5	10.2	10.7	11.3	12.1	13.4
DMC_6 selectivity, mol%									
$2,4DMC_6$	—	23.1	29.5	31.9	32.7	32.7	33.7	34.0	34.9
$2,5DMC_6$	—	76.9	68.7	56.8	46.4	40.5	34.4	32.2	26.0

[a] Products distribution at 523 K, 1 atm, H_2/HC = 60.

TABLE 2

***n*-Octane Conversion on Pt–Pd-ZSM-48[a]**

n-C_8 conversion, %	5.2	10.3	21.0	37.4	59.3	81.6	83.3	86.7	88.0
Cracking selectivity, %	0.4	0.6	1.8	2.4	6.0	8.1	9.9	12.9	17.1
iC_8 selectivity, %	99.6	99.4	98.2	97.6	94.0	91.9	90.0	87.1	82.8
MC_7 selectivity, %	99.6	99.3	97.3	95.7	90.9	85.1	79.9	72.8	65.5
DMC_6 selectivity, %	—	0.1	0.9	1.9	3.0	6.8	10.2	14.3	17.3
MC_7 distribution, mol%									
$2MC_7$	51.7	49.7	47.9	46.4	44.8	44.1	43.4	42.4	41.6
$3MC_7$	40.2	41.9	43.0	43.2	43.8	44.1	44.5	44.9	45.0
$4MC_7$	8.0	8.3	9.1	10.4	11.4	11.9	12.1	12.7	13.4
DMC_6 selectivity, mol%									
$2,4DMC_6$	24.0	31.3	34.2	37.8	39.0	39.8	39.9	39.5	39.5
$2,5DMC_6$	76.0	68.7	57.0	49.2	43.2	35.8	33.8	29.4	25.7

[a] Products distribution at 523 K, 1 atm, $H_2/HC = 60$.

Since trimethyl-branched isomers could not be formed within the SAPO-31 or ZSM-48 channels, cracking reactions involved the β-scission either of monomethylheptanes or of preferably dimethylhexanes. The rates of cracking of the corresponding carbenium ions, which involve secondary → secondary carbenium ion intermediates, are low and are governed by the lifetime of the secondary carbenium ion on the catalyst surface. One should expect that stronger acidity would increase the lifetime of the carbenium ions on the surface, causing enhanced cracking. However, the lifetime of the intermediate carbenium ions on the catalyst surface is probably also governed by the diffusion rates of the products at the pore mouths at a short distance from the external surface. Slow diffusion rates will increase the probability for a cracking event, by β-scission, to occur. The almost identical isomerization selectivity shown by SAPO-31 and ZSM-48 suggests that within constraint materials the restriction to the diffusion of the products out of the pores contributes more to the lifetime of the intermediate carbenium ions than the acid strength. Over narrow-pore molecular sieves, the product distribution from the hydroconversion of *n*-alkanes is a unique function of the molecular sieve topology.

To answer the question to what extent the activity of the narrow-pore molecular sieves in the hydroisomerization reaction would be dependent on the catalyst acidity, the relative rates of the reaction of n-C_8, 2Me-C_7, and 2,2,4TMP over Pt–Pd/SAPO-31 and Pt–Pd-ZSM-48 have been determined. The conversion of the feed was always less than 10%. Table 3 lists the measured relative rates. It is clear that ZSM-48 was more active for hydroconversion of alkanes than SAPO-31. The higher acid strength of ZSM-48 compared to that of SAPO-31 has a beneficial effect on the hydroconversion of *n*-octane and other alkanes. Thus high acidity and narrow nonconnecting tubular pore topology are prerequisites for modeling highly efficient hydroisomerization catalysts.

However, Table 3 shows that 2,2,4TMP, which is indeed too bulky to enter the pores of SAPO-31 or ZSM-48, nevertheless experienced cracking. The main product, more than 95%, was isobutane from β-scission of the 2,2,4-trimethylpentyl carbenium ion.

The reaction of 2,2,4TMP occurred obviously on the catalyst grain surface. Due to its higher acid strength and to the smaller grain size, ZSM-48 exhibited the higher cracking activity. Thus the acid sites on the grain surface participate in the overall hydroconversion of *n*-octane particularly at high conversion where the concentration of methyl-branched C_8 isomers is high. The absence of sterical constraint on the grain surface will permit the formation of multibranched methyl isomers. These multibranched isomers experience rapid cracking by β-scission. The yield of isomerization will thus be lowered. It is thus important to minimize the effect of the external surface of the grains to improve the hydroisomerization selectivity. This may be accomplished by selectively poisoning or removing the acid sites present on the external surface.

The stronger influence of the molecular sieve topology compared to the acid strength on the selective hydroisomerization of alkanes was further studied through the reaction of $2MeC_7$. It has been shown that at low conversion $2MeC_7$ reacted over molecular sieves almost exclusively through hydroisomerization (17). Cracking represented less than 3–4% of the total conversion; similarly the extent of branching rearrangement into dimethylhexanes was low.

TABLE 3

Reaction Rate ($\alpha \times$ WHSV) of C_8 Alkanes over Pt–Pd/ZSM-48 and Pt–Pd/SAPO-31 at 523 K, $H_2/HC = 60$, $\alpha < 10\%$

n-C_8		2Me-C7		2,2,4TMP	
ZSM-48	SAPO-31	ZSM-48	SAPO-31	ZSM-48	SAPO-31
22.2	5.3	75.8	11.6	12.3	2.7

TABLE 4

Reaction of 2Me-C_7 at 523 K over Pt–Pd/Molecular Sieves: Molecular Ratio $3MeC_7/n$-C_8 at Low Conversion <10%

	SAPO-5	SAPO-31	SAPO-41	SAPO-11	ZSM-48	ZSM-22	ZSM-23
Pore size (nm)	0.73	0.54	0.43 × 0.7	0.39 × 0.7	0.55	0.44 × 0.54	0.4 × 0.52
$3MeC_7/n$-C_8	8	3.8	2.3	1.8	2.5	1.2	0.78

The main reactions which occurred were (i) rearrangement with no change of the degree of chain branching through a 1,2-methyl shift which transforms $2MeC_7$ into $3MeC_7$, and (ii) rearrangement with decrease of the degree of branching through a protonated cyclopropane intermediate, $2MeC_7$ being converted into n-C_8. Over a nonconstrained surface, the 1,2-methyl shift is faster than the PCP step; thus, starting from $2MeC_7$ the ratio $3MeC_7/n$-C_8 is in general high, while this ratio decreased as the pore constraint increased (17). In Table 4 are reported the molecular ratios $3MeC_7/n$-C_8 resulting from the reaction of ratio $2MeC_7$ at 523 K over molecular sieve-based bifunctional catalysts.

This table indicates indeed that the isomerization paths, 1,2-methyl shift and PCP, are influenced by the molecular sieve topology rather than by the acidity of the catalyst. Again transition state shape selectivity at the pore mouths prevails over medium tubular pore molecular sieves. The steric constraint exerted on the transition state intermediate is more significant than the acid strength. The ratio $3MeC_7/n$-C_8 would thus follow the pore size rather than the acidity. It is concluded that the smaller the pore size, the lower the ratio of $3MeC_7/n$-C_8. These results suggest that the PCP intermediate can easily be distorted in the catalyst pores, while the 1,2-methyl-shift intermediate will be more rigid. Hence, as the steric constraint increases with the decrease of the pore size the effect on PCP intermediates thus results in the decrease of the $3MeC_7/n$-C_8 ratio. Since the channels in SAPO-31 and ZSM-48 have almost identical sizes, these materials gave a similar ratio $3MeC_7/n$-C_8 upon $2MeC_7$ hydroconversion. These results indicate clearly that the acid strength played a minor role on the isomerization selectivity when compared to the important influence exerted by the dimension and the topology of the molecular sieve channels.

CONCLUSION

The hydroisomerization of long-chain alkanes which is an important class of catalytic reactions is strongly favored over medium-pore noninterpenetrating tubular molecular sieves. The reactions occur inside the pore at the pore mouth at a short distance from the external surface. The hydroisomerization yield is rather high over these materials with preferential formation of monomethyl isomers. The productivity of isomers is considerably increased with an increase in the acidity of the catalysts with little decrease of the selectivity toward isomerization. However, over small grain catalysts the external surface plays a negative role due to the presence of nonselective active sites.

REFERENCES

1. Miller, S. J., *Microporous Mater.* **2**, 439 (1994).
2. Martens, J. A., Parton, R., Uytterhoeven, L., Jacobs, P. A., and Froment, G. F., *Appl. Catal.* **76**, 95 (1991).
3. Miller, S. J., U.S. Patent, 4859311 (1989).
4. Mériaudeau, P., Tuan, Vu A., Lefebvre, F., Nghiem, Vu T., and Naccache, C., *Microporous Mesoporous Mater.* **22**, 435 (1998).
5. Martens, J. A., Souverijns, W., Verrelst, W., Parton, R., Froment, G. F., and Jacobs, P. A., *Angew. Chem. Intern. Ed. Engl.* **34**, 2528 (1995).
6. Souverijns, W., Martens, J. A., Froment, G. F., and Jacobs, P. A., *J. Catal.* **174**, 177 (1998).
7. Mériaudeau, P., Tuan, Vu A., Lefebvre, F., Nghiem, Vu T., and Naccache, C., *Microporous Mesoporous Mater.* **26**, 161 (1998).
8. Hasha, D., Saddalrriaga, L., Hataway, P. E., Cox, D. F., and Davis, M. E., *J. Am. Chem. Soc.* **110**, 2127 (1988).
9. Bennett, J., and Kirchner, R. M., *Zeolites* **12**, 338 (1992).
10. Schlenker, J. L., Rohrbaugh, W. J., Chu, P., Valyocsik, E. W., and Kokotailo, G. T., *Zeolites* **5**, 355 (1985).
11. Müller, D., Jahn, E., Fahlke, B., Ladwig, G., and Haubenreisser, U., *Zeolites* **5**, 53 (1985).
12. Martens, J. A., Grobet, P. J., and Jacobs, P. A., *J. Catal.* **126**, 299 (1990).
13. Jahn, E., Müller, D., and Becker, K., *Zéolites* **10**, 151 (1990).
14. Frende, D., Ernst, H., Hunger, M., Pfeifer, H., and Jahn, E., *Chem. Phys. Lett.* **143**, 477 (1998).
15. Blackwell, C. S., and Patton, R. L., *J. Phys. Chem.* **88**, 6135 (1984).
16. Zibrowius, B., Löffler, E., and Hunger, M., *Zeolites* **12**, 167 (1992).
17. Martens, J. A., Mertens, M., Grobet, P. J., and Jacobs, P. A., *Stud. Surf. Sci. Catal.* **37**, 97 (1988).
18. Lugstein, A., Jentys, A., and Vinek, H., *Appl. Catal. A* **166**, 29 (1988).